



Contents lists available at ScienceDirect

Ocean Modelling

journal homepage: www.elsevier.com/locate/ocemod

Refined source terms in wind wave models with explicit wave breaking prediction. Part I: Model framework and validation against field data

Michael L. Banner*, Russel P. Morison

School of Mathematics and Statistics, The University of New South Wales, Sydney 2052, Australia

ARTICLE INFO

Article history:

Received 23 May 2009

Received in revised form 24 November 2009

Accepted 11 January 2010

Available online xxx

Keywords:

Wind waves

Wind wave modelling

Wave breaking

Breaking wave forecasts

ABSTRACT

Wave breaking in the open ocean is a widespread air–sea interfacial process with very significant geophysical and maritime importance, yet present spectral wave forecast models do not provide explicit forecasts of breaking wave properties. Recent advances in understanding the wave breaking process have made it possible to redress this deficiency.

This paper describes a novel methodology that adds accurate forecasts of the spectral density of breaking crest length per unit area and associated breaking strength for the dominant wind waves to standard directional wave height spectrum forecasts.

A threshold-based formulation for the breaking component of the dissipation rate source term is proposed within a broad bandwidth spectral wind wave model. An ‘exact’ form of the nonlinear source function was used to avoid spurious effects arising from faster approximate versions for this source term. A spectral wind input formulation compatible with these two source terms was chosen from the suite of existing forms. Our model was required to reproduce measured dimensionless energy evolution, mean squared slope, directional spreading, wind stress and total water-side dissipation rates. In addition, we sought to match modelled and observed breaking properties. This large set of constraints required a critical reassessment of the strengths of the wind input and dissipation rate source terms relative to the nonlinear spectral transfer term.

Detailed comparisons are made between the model predictions and results from the unique FAIRS open ocean data set where breaking wave observations were gathered along with wind stress, wave height and water-side dissipation rate measurements. The model results closely reproduced the observed breaking wave properties in addition to the characteristics listed above.

© 2010 Published by Elsevier Ltd.

1. Introduction

Over the past decade, knowledge of the marine boundary layers adjoining the air–sea interface has advanced significantly. On the water side, turbulent kinetic energy (TKE) dissipation rate measurements have revealed greatly enhanced levels over conventional rough wall estimates (e.g. Terray et al., 1996). From the surface-following dissipation rate measurements of Gemmrich and Farmer (2004), this enhancement is clearly attributable to wave breaking. Also, in the atmospheric boundary layer, wave breaking was found to increase the drag coefficient (Babanin et al., 2007). According to Donelan (1998), most of the wind input momentum and energy fluxes to the waves leave the wave field locally via wave breaking to drive currents and generate turbulence, respectively, in the upper ocean. This implies that dissipation through wave breaking is a key process in the evolution of wind

waves. Wave breaking also produces a complex overturning of the sea surface, leading to enhanced interfacial fluxes (e.g. Melville, 1994). Even on basin-wide scales, recent theoretical model studies have demonstrated potentially strong contributions from breaking waves to the circulation and mixing (e.g. Restrepo, 2007, among others). Yet, in the context of wave forecasting models, the dissipation rate remains the least well-understood source term relative to the other two source terms, wind input and nonlinear spectral transfer.

Wave breaking in deep water is associated with wave energy focusing (convergence), and often occurs at envelope maxima of wave groups (Donelan et al., 1972; Holthuijsen and Herbers, 1986). Further, evidence is building that wave breaking in deep water is a process with a generic threshold that reflects the convergence rate and geometrical steepening of the waves that break. From their innovative analysis of storm waves, Banner et al. (2002) reported that a parameter based on the wave spectral saturation (Phillips, 1985) provides a robust spectral breaking threshold, at least for waves in the energy-containing range. It should be noted that the background turbulence in the wave boundary

* Corresponding author.

E-mail addresses: m.banner@unsw.edu.au, mlb2121@columbia.edu (M.L. Banner).

layer, to which breaking waves of all scales contribute, also has a role in dissipating the energy of wind waves. This has been highlighted in the context of swell attenuation (e.g. Teixeira and Belcher, 2002; Ardhuin and Jenkins, 2006), but is surely operative during active wind wave generation.

The highly nonlinear nature of breaking in physical space presents very substantial challenges for modelling this process in the phase-unresolved spectral domain used in contemporary wind wave models. Nevertheless, the observational perspective described in the opening paragraph provides a strong motivation for seeking a plausible modelling framework for representing the effects of wave breaking at different spectral scales. Based on recent field observations, refinements of the source terms for wind input and dissipation rate are proposed. This refined suite of source terms provides more accurate and informative severe sea state forecasts that include the breaking properties of the dominant waves.

This paper describes the underlying methodology, which synthesises several aspects of new knowledge about wave breaking gained from our recent studies. A detailed validation is reported against data from the recent FAIRS experiment, described in Section 2.1.2. A companion paper addresses the validity of this model over a wide range of wind speeds from light to hurricane strength.

2. Observational background

While wave breaking remains incompletely understood, there has been exciting progress in recent years. From both laboratory and field studies, a major observational advance on deep water wave breaking onset was identifying it as a strongly thresholded process, with a threshold based on a suitable measure of wave non-linearity. Recent numerical and laboratory studies of narrow band wave packets have also provided encouraging progress on understanding the closely linked issue of breaking strength, which has proven to be more elusive to quantify in field studies. These advances have underpinned the development of the present modelling framework that includes predictions of wave breaking properties in sea state forecast models.

Breaking of deep water waves is linked to excess energy convergence to the waves that break, which can occur via a number of mechanisms. In one representative breaking scenario, the recent laboratory studies of Banner and Peirson (2007) and Tian et al. (2008) investigated the evolution of unidirectional weakly nonlinear wave packets. These studies reported a strong correlation of breaking onset and breaking energy loss on the convergence rate parameter proposed by Song and Banner (2002). After its initiation, breaking was observed to recur at successive wave group maxima, as noted decades earlier in field observations by Donelan et al. (1972). This aspect of the breaking process has received scant attention, yet it can have significant implications for recent observational field studies targeting $\mathcal{A}(c)$, the spectral density of breaking crest length per unit sea surface area. This framework, which uses the speed of the breaking wave front as a measure of the scale of breaking, was introduced by Phillips (1985) and is described in the following paragraph. Recent advances in measurement techniques have facilitated initial field measurements of $\mathcal{A}(c)$, a challenging task over the open ocean.

The spectral measure of breaking waves, $\mathcal{A}(c)$, has the property that $\mathcal{A}(c) dc$ gives the mean crest length per unit sea surface area, of breaking crests travelling with velocities in $(c, c + dc)$. $\mathcal{A}(c)$ is one of the primary breaking forecast parameters computed in this study. $\mathcal{A}(c)$ can also be used to model breaking wave enhancements to the wind stress and allied air–sea fluxes such as sea spray based on the sea state, rather than just the wind field.

Relating geometric/kinematic measurements of $\mathcal{A}(c)$ accurately to the underlying energy dissipation rate $\varepsilon(c)$ is a major challenge.

Phillips (1985, Eq. (6.3)) proposed the following connection between these two distributions, given below in scalar form:

$$\varepsilon(c) dc = b g^{-1} c^5 \mathcal{A}(c) dc \quad (1)$$

where the non-dimensional coefficient b connects the energetics to the breaking geometry and kinematics, and reflects the breaking strength.

Underlying (1) is the assumption that the mean wave energy dissipation rate at scale $(c, c + dc)$ is dominated by wave breaking at that scale. This may have shortcomings, especially for shorter breakers due to the attenuation of short wave energy by the passage of longer breaking waves (e.g. Banner et al., 1989). A less restrictive form for S_{ds} should have a local contribution from the given breaking wave scale, S_{ds}^{loc} , plus a background attenuation component, S_{ds}^{nlc} , representing the background turbulence in the wave boundary layer and the cumulative attenuation of short waves by longer breaking waves sweeping through them. To account for these effects, we modelled the total dissipation rate as the sum of these two contributions:

$$S_{ds} = S_{ds}^{loc} + S_{ds}^{nlc} \quad (2)$$

The forms adopted in this study for these terms are described in Section 3.4.

It is noted that the limited open ocean data for $\mathcal{A}(c)$ reported to date do not provide an unambiguous trend towards shorter scales, as discussed below. The image processing techniques used by various authors were quite distinct, and we were not able to reconcile the reported differences. Hence in this study while breaking occurs across the spectrum, we decided to focus on predicting the breaking of the waves at the spectral peak. These dominant waves are likely to be the most energetic breaking wave scale in growing seas as well as in very severe sea states where they are strongly forced by the wind.

The dependence of breaking strength b on wave variables is not well understood. The expectation is that b should increase systematically with wave nonlinearity. Banner and Peirson (2007) reported direct measurements of b values for laboratory spilling breakers that increase linearly from 8×10^{-5} to 1.2×10^{-3} as the convergence rate parameter increased. The very recent laboratory study of Tian et al. (2008) also reported similar levels for b .

Initial field measurements of \mathcal{A} and b were published by Phillips et al. (2001) and Melville and Matusov (2002). In addition to concerns about certain aspects of the data processing in these studies, these data sets were gathered only during fully developed sea states. For model validation, data for growing seas as well as developed wind seas were needed. The only such data known to us was collected from RV FLIP in October 2000 during the FAIRS (Fluxes, Air–Sea Interaction and Remote Sensing) project. That data was analysed by Gemmrich et al. (2008), who reported measurements of $\mathcal{A}(c)$ and the mean breaking strength $\langle b \rangle$ averaged across the wave spectrum. While the range of wave age conditions is rather limited, these results provide a valuable initial validation source for our model performance. In regard to the short breaking waves in the spectral tail, Melville and Matusov (2002) show $\mathcal{A}(c)$ increasing towards smaller c values, while Gemmrich et al. (2008) report a very strong attenuation of breaking waves for speeds below about $0.2c_p$, where c_p is the speed of the spectral peak waves. This is evident in their Fig. 2, and needs to be clarified in future studies.

2.1. Recent wave breaking field observations

2.1.1. Breaking probability in the spectrum

Banner et al. (2000) found a significant correlation for the breaking probability of the dominant wind waves with the peak

wave steepness, operative once a threshold significant steepness level had been exceeded. In our spectral breaking wave forecast model framework, a breaking criterion also applicable to waves shorter than the dominant waves was sought to be able to include breaking wave effects associated with shorter wave scales.

From their analysis of storm wave data sets, Banner et al. (2002) reported a high correlation of breaking probability with the spectral saturation $B = k^4 \Phi(\mathbf{k}) = (2\pi)^4 \int^{\infty} F(f)/2g^2$ for wave scales from the spectral peak frequency f_p out to $2.5f_p$, and demonstrated a very strong threshold behaviour. After normalisation to allow for the growing directional spreading of the waves with f/f_p , they found that the saturation breaking threshold is almost constant across the above observed frequency range of $1 < f/f_p < 2.5$. This is seen in Fig. 7 in Banner et al. (2002). That result formed the basis of our formulation of the spectral wave breaking dissipation rate source term, which underpins our calculation of breaking crest length spectral density and breaking strength.

2.1.2. Observational results from the FAIRS experiment

The data analysis methodology for the breaking crest spectral density distributions used to validate this study was reported in Gemmrich et al. (2008). In brief, the FAIRS experiment took place during September–October 2000 from the research platform FLIP, roughly 150 km off Monterey, California. Two downward looking monochrome video cameras mounted on the face boom recorded whitecap events. There were synchronous measurements of wind speed and direction, wind stress and wave height. Fig. 1 summarises the observed conditions and salient data. This unique data set includes wave breaking measurements for a developing wind sea ($U_{10}/c_p \sim 1.09$), in addition to mature sea conditions ($U_{10}/c_p \sim 0.81$). Such data for developing wind seas were not previously available. Here, developing sea ($U_{10}/c_p \sim 1.09$) is denoted period 1, and mature sea ($U_{10}/c_p \sim 0.81$) is denoted period 3. Also indicated in Fig. 1 are periods 2 and 4. These refer to aging seas and a newly developing mixed sea event during the FAIRS observational period, but were not used in this study.

Fig. 2 summarises the differences in the measured probability distribution of breaking waves with wave speed histograms for developing seas ($U_{10}/c_p \sim 1.09$) and mature seas ($U_{10}/c_p \sim 0.81$). The crucial feature evident for the *developing* seas (period 1) is that breaking occurs around the spectral peak, as well as for the shorter

waves. However, there is no breaking of the spectral peak waves for the mature seas in period 3. It is noted that in most forms of the wind input source term, there is relatively low wind input to the spectral peak waves for $U_{10}/c_p \sim 1.09$, yet the observations confirm the presence of dominant wave breaking, as measured directly by the breaker speeds close to the dominant wave speed c_p . Hence these are not shorter waves that break at the crests of dominant waves.

This figure also indicates a pronounced fall-off in the breaking wave probability distribution as c decreases below about $\sim(0.2-0.3)c_p$. This does not appear to be due to resolution limitations of the observations. As the underlying physics is not well understood, we have focused our attention on the dominant breaking waves, seeking to forecast their geometrical distribution and strength for different wind speed and wave age conditions. Refining our modelling framework for the short breaking waves is left to the future when their physics is better understood.

2.2. Modelling objectives

The availability of co-located open ocean breaking wave data has contributed significantly to extending existing benchmarks for accurate wind wave model predictions. Our extended set of benchmarks comprises:

- Reproducing the evolution trajectories of non-dimensional mean wave energy E and spectral peak frequency f_p .
- Reproducing key spectral tail properties: mean directional spreading with k/k_p ; spectral saturation; level and exponent of 1D transect k -spectrum (k is the wavenumber, k_p is the spectral peak wavenumber); slice in the wind direction of the directional wavenumber spectrum.
- Validating relative levels of the computed wave-induced stress (non-breaking and breaking) relative to overall wind stress driving the model.
- Predicting breaking crest length/unit area spectral density λ and breaking strength b at different wave ages.
- Ensuring model-generated integrated water-side dissipation rates match observed levels, and are consistent with the integrated energy flux from the wind to the waves.

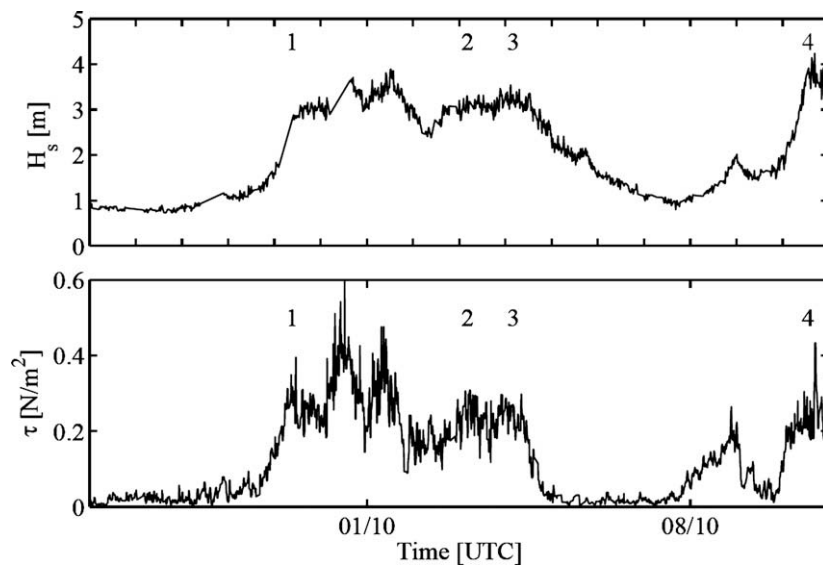


Fig. 1. Significant wave height (H_s), wind stress τ during the FAIRS experiment. The wind direction was around 300° for most of the observational period. Periods 1 (growing seas) and 3 (mature seas) are of particular interest in this study, during which the observed mean wind speed was 12 m/s. Periods 2 and 4 refer to aging seas and a newly developing mixed sea event during the FAIRS observational period, but these were not used in this study.

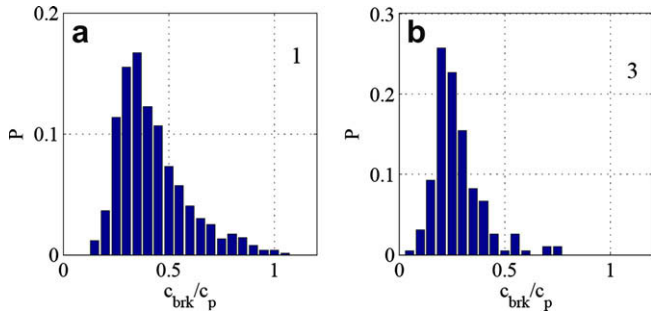


Fig. 2. Probability distribution of breaking waves as a function of wave speed relative to the spectral peak, for period 1 (growing seas) and 3 (mature seas). Note that breaking events occur in the spectral peak region for period 1, but not for period 3. Also note the rapid fall-off of breaking towards the shortest wave scales.

Our goal in this study was to reproduce the observed properties in A–E above using numerical forecasts based on our wind wave model source terms, as described in Section 3.

3. Overview of wind wave modelling approach

3.1. Radiative transfer equation

The evolution of the wave height spectrum was computed via the radiative transfer equation (Komen et al., 1994) assuming deep water and negligible currents:

$$\frac{\partial \Phi}{\partial t} + \mathbf{c}_g \cdot \nabla \Phi = S_{\text{tot}} \quad (3)$$

where $\Phi = \Phi(k, \theta)$ is the directional wave spectrum and \mathbf{c}_g is the group velocity. The total source term $S_{\text{tot}} = S_{\text{in}} + S_{\text{nl}} + S_{\text{ds}}$, where S_{in} is the atmospheric input spectral source term, S_{nl} is the nonlinear spectral transfer source term representing nonlinear wave–wave interactions and S_{ds} is the spectral dissipation rate, primarily due to wave breaking.

3.1.1. Spectral bandwidth of the calculations

We ran broad spectral bandwidth computations of the evolution of the directional wave spectrum including the tail using an ‘exact’ version of the nonlinear wave–wave interaction source term S_{nl} in the radiative transfer equation (3) (e.g. see Eq. (2.145) in Komen et al., 1994). In our calculations, a logarithmic grid was used to accommodate the evolution from very young to very old wind seas over the wide range of wind speeds we investigated.

From the outset we required that S_{ds} and S_{in} should not be compromised by approximations in S_{nl} . The ‘exact’ form of S_{nl} was used to avoid the often poor approximation to the full S_{nl} term calculation provided by the ‘discrete interaction approximation’ (DIA) implementations currently in use operationally (e.g. see III.3.2 in Komen et al., 1994; Resio and Perrie, 2008).

The consequence of using an ‘exact’ form of S_{nl} was very long computational times, due to the millions of interactions that need to be calculated at each space or time step in the evolution. This effect becomes more pronounced at higher wind speeds, where the time or space step needed to be shortened for stability, with model runs at hurricane wind speeds requiring up to several days to reach notionally ‘mature’ conditions where the dominant wave speed was close to the 10 m wind speed.

In our validations, we concentrated on duration-limited growth cases, which are the least prone to spurious numerical instability. There are established non-dimensional duration-limited growth correlations for wave energy and peak frequency based on field observations (Young, 1999). These can also be inferred from fetch-limited observations by the methodology discussed in

Hwang and Wang (2004). This ensures that modelled spectral saturation levels, and hence dissipation rates, are consistent with observed levels.

3.2. Wind input source term S_{in}

The magnitude and spectral composition of the wind input source term S_{in} remains imprecisely known, despite very considerable observational and theoretical study over the past few decades. In the context of developing a model framework for forecasting breaking properties, we investigated a number of proposed S_{in} formulations. We found a number of the formulations were so strong in the peak region, that the modelled drag coefficients were much too high and dwarfed the S_{nl} and corresponding S_{ds} levels, which narrowed the direction spreading to well below observed levels. These forms include Yan (1987) and Tolman and Chalikov (1996). These forms of S_{in} were not explored further in our analysis. We also made a detailed study of the Hsiao and Shemdin (1983) form for S_{in} . This is very low in the peak region, and very strong in the tail, relative to other input terms. Using this form we were unable to generate sufficient input to match reasonable dissipation levels in the peak region, whereas the input in the tail was so strong, that corresponding drag coefficients were well above those observed. For intercomparison, Fig. 3 shows the non-dimensional growth rates γ for these various forms of S_{in} for a developing wind sea. Note that these different forms of S_{in} can differ considerably (the ordinate is logarithmic) as regards their spectral levels for both long and short wave components.

The form of the wind input S_{in} that appeared to come closest to matching the available observations was Janssen (1991), although the tail levels were a little strong, and the peak levels a little weak, especially in higher wind speeds. Janssen (1991) is based on the critical layer theory of Miles (1957) and is tuned closely to available field measurements of Snyder et al. (1981) and laboratory measurements (Plant, 1982). The differences between these are indicative of the level of uncertainty between nominal S_{in} forms used in different contemporary wave models.

We made a modification to the Janssen (1991) input source term in the spirit of the notion of sheltering (e.g. Belcher and Hunt, 1993; Makin and Kudryavtsev, 2001; Hara and Belcher, 2002; among others). This reduces the driving stress to the shorter waves by subtracting the fraction of the wave stress supported by the longer waves. It allowed us to fine tune the integrated wind input energy flux to balance the integrated energy loss rate due to breaking. This is an important validation check for the modelling, and we also found that our sheltering algorithm provided wind stress estimates that agreed closely with observed levels as the wind sea aged.

3.2.1. Sheltering strategy

The total aerodynamic drag is the sum of the wave drag, the breaking wave drag and the tangential stress, i.e.

$$\tau_{\text{tot}} = \int \tau_w(k) dk + \int \tau_{\text{bw}}(k) dk + \tau_{\text{tang}} \quad (4)$$

The wave stress is expressed as

$$\tau_w(k) = \rho_{\text{air}} \int \alpha(\Phi(k, \theta)/c) k d\theta \quad (5)$$

where the growth rate α is given below.

The breaking wave stress is expressed as

$$\tau_{\text{bw}}(k) = Pr_{\text{br}}(k) * \chi(k) * \tau_w(k) \quad (6)$$

where $Pr_{\text{br}}(k)$ is the breaking probability at scale k and $\chi(k)$ is the ratio of actual crests to Fourier modes at scale k . For details on

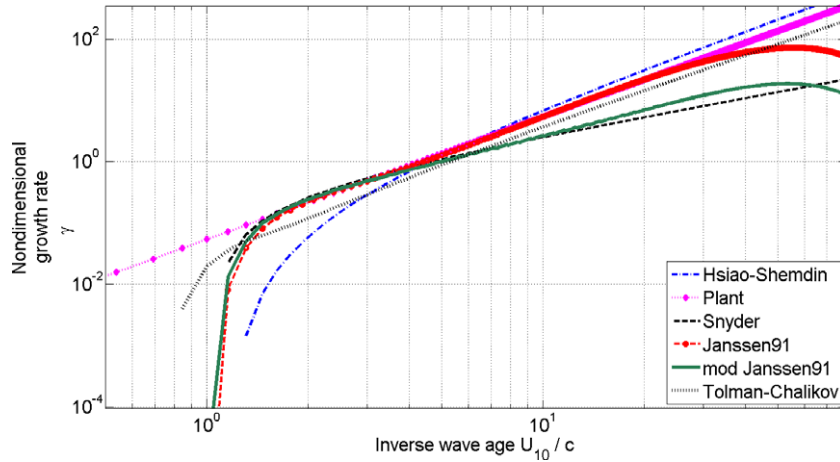


Fig. 3. Logarithmic plot highlighting the considerable differences between the spectral growth rate γ of selected commonly implemented forms of S_{in} for maturing seas ($U_{10}/c_p \sim 1.0$). The modified Janssen91 curve shows the extent of sheltering introduced for the slower moving, shorter wave components. This is sufficient to align the computed wind stress with observed levels.

how $Pr_{br}(k)$ and $\chi(k)$ are defined and parameterised based on observations, see Section 3.5.

The tangential stress parameterisation is expressed as

$$\tau_{tang} = A\rho_{air}U_{10}^2 \quad (7)$$

with $A = \max [10^{-5}, 1/(t_1 U_{10}^2)]$, where $t_1 = 325$ and $t_2 = 0.9$.

This was based on the tangential drag coefficient behaviour reported by Banner and Peirson (1998). They observed that the tangential drag coefficient was a decreasing function of the wind speed, largely independent of the wave age. Our parameterisation conforms to their data trend at moderate wind speeds, and asymptotes to a residual level for the drag coefficient of 10^{-5} for hurricane conditions. It is assumed that no matter how strong and widespread the air flow separation becomes, the wind always maintains some residual re-attachment to the water surface, where the tangential stress will be small, but non-zero.

In the present modelling, the overall friction velocity is given by $u_* = \sqrt{\tau_{tot}/\rho_{air}}$. Also, the reduced friction velocity $u_*^{red}(k_n)$ felt by the n th wavenumber k_n , which reflects the sheltering of the short waves by the longer waves, is given by

$$u_*^{red}(k_n) = \sqrt{\left[\tau_{tot} - c_r \sum_{i=1}^n (\tau_w(i) + \tau_{bw}(i)) \right] / \rho_{air}} \quad (8)$$

for $1 \leq n \leq N$, where N is the total number of wavenumber grid points. We set $c_r = 0.95$ to ensure that the reduced u^* does not become too small, especially at high wind speeds. Note that $i = 1$ corresponds to the lowest wavenumber, so as k_n increases, the cumulative effect of wavenumber contributions to the wave stress is felt increasingly. At each time step, the model recalculates the total u^* and the reduced u^* , given by (8), which are then fed back into the wind input source term. This key aspect of the wind input source term is described in the following section.

3.2.2. Modified Janssen (1991) wind input growth rate formulation

Based on Janssen (1991), we define

$$\mu(k, \theta) = (u_*/c)^2 (gz_0/u_*^2) \exp(J_1 \kappa / (u_* \cos \theta / c)^2) \quad (9)$$

where $\kappa = 0.4$ is the Karman constant, c is the phase speed and θ is the direction of the waves relative to the wind and $J_1 = 0.99$ (Janssen (1991) used $J_1 = 1$). The roughness length z_0 follows the form proposed by Janssen (1991):

$$z_0 = \frac{0.01u_*^2}{g} \sqrt{1 - c_0(\tau_w/\tau)} \quad (10)$$

where c_0 was set at 0.8 to ensure that the denominator did not become excessively small.

The Miles parameter is given by

$$\begin{aligned} \beta(k, \theta) &= J_2 \mu (\ln(\mu))^4 / \kappa^2 \quad \text{where } J_2 = 1.6 \text{ (Janssen (1991) used 1.2)} \\ \beta(k, \theta) &= 0 \quad \text{for } \mu > 1 \end{aligned} \quad (11)$$

The modified Janssen spectral growth rate is then given by

$$\alpha(k, \theta) = \varepsilon \beta(k, \theta) \omega (u_*^{red}(k) \cos \theta / c)^2 \quad (12)$$

where ε is the ratio of air to water densities, and the corresponding wind input source term is

$$S_{in}(k, \theta) = \alpha(k, \theta) E(k, \theta) \quad (13)$$

Note that the form of Janssen's growth rate parameterisation has been followed, with the Miles coupling parameter based on the overall u^*/c but the input to the shorter waves has been modified by using u_*^{red} in the quadratic forcing term.

The modified input growth rate used in our calculations is shown in Fig. 3 for a maturing sea state with wave age $c_p/U_{10} = 1$.

3.3. Nonlinear spectral transfer source term S_{nl}

Before proceeding with our investigation of S_{ds} , various versions of the 'exact' S_{nl} code and propagation/stepping schemes were tested to ensure accuracy and minimise computational instabilities that can develop at higher wavenumbers. The version of S_{nl} we used is a recent update (Resio, private communication) of Tracy and Resio (1982) that has directional coverage of $\pm 180^\circ$. We verified that the 'exact' nonlinear transfer term has zero net integral at all times.

3.4. Spectral dissipation rate term S_{ds}

We used a spectral saturation-based form of S_{ds} that has evolved substantially from the form proposed by Alves and Banner (2003). This form was originally motivated by the observed strong threshold behaviour reported by Banner et al. (2002) for the wave breaking probability in the spectrum, Pr_{br} . This is defined as the ratio of the passage rate past a fixed point of breaking crests with

speeds in $(c, c + dc)$ to the passage rate past a fixed point of all wave crests with speeds in $(c, c + dc)$.

The sea state threshold variable used was the normalised spectral saturation

$$\bar{\sigma}(k) = \sigma(k) / \langle \theta(k) \rangle \quad (14)$$

where $\sigma(k)$ is the azimuth-integrated spectral saturation given by

$$\sigma(k) = k^4 \Phi(k) = (2\pi)^4 f^5 G(f) / 2g^2 \quad (15)$$

and $\langle \theta(k) \rangle$ is the mean spectral spreading width given by

$$\langle \theta(k) \rangle = \int_{-\pi}^{\pi} (\theta - \bar{\theta}) F(k, \theta) k d\theta / \int_{-\pi}^{\pi} F(k, \theta) k d\theta \quad (16)$$

where $\bar{\theta}$ is the mean wave direction, and $\Phi(k)$, $G(f)$ and $F(k, \theta)$ are, respectively, the spectra of wave height as a function of scalar wavenumber, frequency and vector wavenumber.

The observed breaking probabilities for different centre frequencies relative to the spectral peak were then found to have a well-defined threshold behaviour, with a common breaking threshold value $\bar{\sigma}_T \sim 0.0045$ (Banner et al., 2002).

Based on the strongly thresholded behaviour indicated by these observations of breaking probability, we reformulated the S_{ds} term proposed by Alves and Banner (2003). The new form embodies normalised saturation threshold behaviour, based on treating waves in different directional spectral bands as nonlinear wave groups. It is in the spirit of the nonlinear forms of S_{ds} discussed by Donelan and Yuan in §II.4 of Komen et al. (1994).

The form of S_{ds} used in this study is

$$S_{ds}(k, \theta) = S_{ds}^{loc}(k, \theta) + S_{ds}^{nloc}(k, \theta) \quad (17)$$

$$\text{where } S_{ds}^{loc}(k, \theta) = C_1 Q F_1(\bar{\sigma}) F_2(\sigma) \omega F(k, \theta) \quad (18)$$

$$\text{and } S_{ds}^{nloc}(k, \theta) = C_2 Q F_2(\sigma) \omega F(k, \theta) \quad (19)$$

$$\text{Here } F_1(\bar{\sigma}) = \begin{cases} ((\bar{\sigma} - \bar{\sigma}_T) / \bar{\sigma}_T)^{a_1} & \bar{\sigma} > \bar{\sigma}_T \\ 0 & \bar{\sigma} \leq \bar{\sigma}_T \end{cases} \quad (20)$$

$$\text{and } F_2(\sigma) = \begin{cases} (\sigma / \sigma_m)^{a_2} & k > k_m \\ 1 & k \leq k_m \end{cases} \quad (21)$$

In these expressions, σ and $\bar{\sigma}$ are the saturation and the saturation normalised by the directional spreading width, $\bar{\sigma}_T$ is threshold normalised saturation and σ_m is the saturation at k_m , the mean wavenumber at the transition between the peak enhancement region and the spectral tail. Typically, this transition wavenumber is located at $k_m \sim 1.5k_p$. The breaking threshold switch exponent a_1 was taken as 2 and the exponent a_2 was taken as 4, based on matching to the high wavenumber form of $S_{in}(k)$. The normalised spectral saturation is smoothed to decrease the effect of very strong gradients in the region of the spectral peak, and has little effect elsewhere in the grid. The smoothed saturation is used in both the dissipation source term, and in calculating breaking probabilities.

For the integrated wave spectrum, the difference between the integrated wind input and integrated dissipation rates determines the overall energy growth (see Fig. 4b). As the wind input growth rate is approximately a quadratic function of the wind speed, the corresponding dissipation rate S_{ds}^{loc} also needs to have a similar dependence. The close to linear dependence of the mean square slope (mss) on wind speed combines with the quasi-linear wind speed dependence of the saturation terms to produce a dissipation rate depending on wave field variables that is approximately quadratic in the wind speed. This requirement was achieved setting Q in (18) and (19) to the SOWEX form of the mss (Eq. (25) in Banner et al., 1999), raised to the power 5/4. This form for the mss is based

on a 25-mm water wavelength cutoff. Full optical bandwidth mss dependence parameterisations (Cox and Munk, 1954; Br on and Henriot, 2006) could equally well have been used. The coefficients $C_1 = 1.25 \times 10^{-3}$ and $C_2 = 4 \times 10^{-4}$ were tuned to provide the optimal match over a wide range of wind speeds to observed duration evolution data of the spectral peak energy and peak frequency (e.g. Young, 1999). This parametric approach was taken in strong preference to direct calculation of the mss due to the use of an appended tail and non-fixed computational bandwidth associated with the intended variable grid geometry in the model.

Finally, S_{ds}^{nloc} is a background turbulence dissipation term that is consistent with observed decay rates of swell propagating over large distances from storm centres. Its form has been the subject of renewed interest (e.g. Teixeira and Belcher, 2002; Arduin and Jenkins, 2006). These authors have developed and refined formulations for this term primarily to address the attenuation of the dominant swell waves that emanate from storm centres and often propagate for vast distances across ocean basins. However, this term also plays a role in the non-local damping of short wind waves, as discussed above.

We investigated using Eq. (15) in Arduin and Jenkins (2006) as a possible candidate for S_{ds}^{nloc} , which predicts an asymptotic high wavenumber behaviour of $k^{-1.5}$. However, this exponent is considerably larger than the wind input spectral tail falloff. Hence imposing this form for S_{ds}^{nloc} over the spectral tail region would be incompatible with the overall dissipation rate consistent with the adopted source terms, which have been tuned to match the wind stress and dissipation rate.

In summary, our proposed form of S_{ds} specified by (17)–(21) based on the (smoothed) local saturation ratio refines the bulk wave steepness threshold used in the quasi-linear form of S_{ds} due to Komen et al. (1994) presently used in most operational wave models.

3.5. Extraction of breaking wave properties: breaking crest length $\Lambda(c)$ and breaking strength b

The relationship (1) proposed by Phillips (1985) relates observed mean geometrical properties of breakers travelling with different speeds to the upper ocean spectral dissipation rate. The $S_{ds}(c)$ used here is related to Phillips (1985) form by $\varepsilon(c) = g S_{ds}(c)$, and only the subcomponent S_{ds}^{loc} in (2) is related to wave breaking. The form of (1) consistent with this is given by:

$$S_{ds}^{loc}(c) dc = b g^{-2} c^5 \Lambda(c) dc \quad (22)$$

where the breaking strength coefficient b implicitly has a dependence on c . In regard to the general applicability of (22) across all wave scales, the discussion following Eq. (1) in Section 2 points out the potential oversimplifications inherent in (1) and (22) for waves shorter than the spectral peak waves. The relationship (22) above relates observed mean geometrical properties of whitecaps travelling with different speeds to the upper ocean spectral dissipation rate S_{ds}^{loc} . However, the dependence of the breaking strength coefficient b in (22) on wave variables is not yet known. In a recent laboratory study on weakly nonlinear wave groups (narrow spectral wave bandwidth), Banner and Peirson (2007) found a strong correlation between b and the energy convergence rate within weakly nonlinear wave groups. A robust parameterization of b for different wind speed and wave ages field conditions for a broad spectral bandwidth of waves, not previously available, is proposed here.

In Banner et al. (2002), the breaking probability at scale c is defined as follows. If $\Lambda(c)$ is the spectral density of breaking wave crest length per unit area with velocities in the range $(c, c + dc)$, then the passage rate of breaking crests in $(c, c + dc)$ past a fixed point is $c \Lambda(c) dc$. The analogous concept of the spectral density of

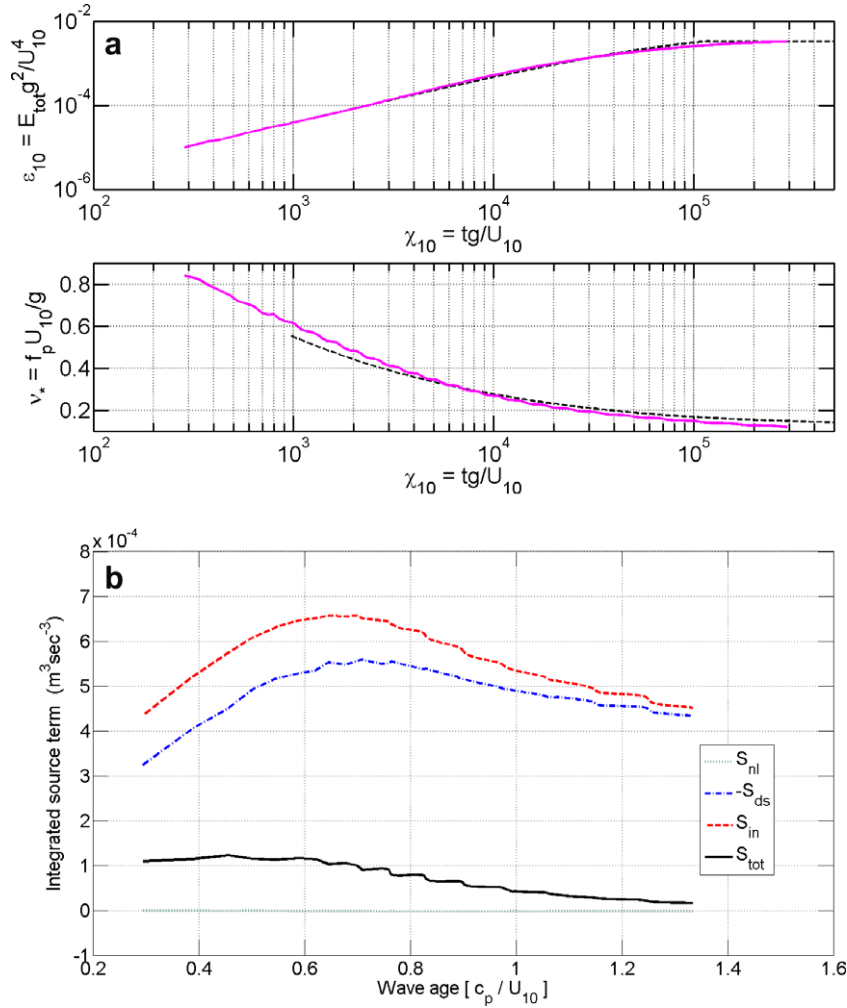


Fig. 4. (a) Evolution of non-dimensional mean wave energy (upper panel) and spectral peak frequency (lower panel) against non-dimensional time for duration-limited growth. The background dashed lines are the trends of the data collated by Young (1999). (b) Evolution of the integrated source terms.

the total wave crest length per unit area $\Pi(c)$ gives the *total* crest passage rate in $(c, c + dc)$ past a fixed point as $c\Pi(c) dc$. The breaking probability $Pr_{\text{br}}(c)$ for wave scales c is defined as:

$$Pr_{\text{br}}(c) = \frac{\int c \mathcal{A}(c) dc}{\int c \Pi(c) dc} \quad (23)$$

Analogous azimuth-integrated forms of \mathcal{A} and Π with scalar independent variables c (phase speed), k (wavenumber magnitude), or f (frequency) are easily defined. The azimuth-integrated version is used here.

A major result from Banner et al. (2002) was that the breaking probability was found to be well-approximated over the spectral range $1 < f/f_p < 2.5$, by a thresholded linear function of the normalised saturation:

$$Pr_{\text{br}}(\tilde{\sigma}) = H(\tilde{\sigma} - \tilde{\sigma}_T) * \alpha_{\text{br}} * (\tilde{\sigma} - \tilde{\sigma}_T) \quad (24)$$

where $\tilde{\sigma}_T = 4.5 \times 10^{-3}$ is the measured normalised spectral saturation breaking threshold. Also, $\alpha_{\text{br}} \sim 33$ is the measured gain of the linear relationship shown in Fig. 7 in Banner et al. (2002), and H is the Heaviside step function.

The breaking probabilities shown are the measured statistics, based on the detected breaker and dominant wave passage rates in the $0.7 < f/f_c < 1.3$ spectral band, where f_c is the centre frequency in the selected band. This is equivalent to $1.43 > c/c_p > 0.77$. It was reported (Fig. 3, Banner et al., 2002) that the actual mean total crest

passage rate for this bandwidth at the spectral peak was a fraction $\gamma \sim 0.6$ of the expected value f_p based on Fourier modes. This empirical result provides a framework for relating modelled spectral peak levels of S_{ds} and $\tilde{\sigma}$ to the corresponding \mathcal{A} and b levels, which are then linked to the nominated spectral peak bandwidth.

Applying the transformed scalar wavenumber form of (22) at the spectral peak gives:

$$b_p \mathcal{A}(k_p) = \frac{g^2}{c_p^5} S_{\text{ds}}^{\text{loc}}(k_p) \quad (25)$$

To recover $\mathcal{A}(c)$ and b from the model output of spectral dissipation rate $S_{\text{ds}}(\mathbf{k})$ and normalised saturation $\tilde{\sigma}$, we use (22)–(25). From (25):

$$b_p = \frac{g^2}{c_p^5} S_{\text{ds}}^{\text{loc}}(k_p) / \mathcal{A}(k_p) \quad (26)$$

$\mathcal{A}(k)$ can be transformed to $\mathcal{A}(c)$ via the linear dispersion relation $c^2 = g/k$, from which

$$\mathcal{A}(k_p) = \mathcal{A}(c_p) c_p^3 / 2g \quad (27)$$

In the azimuth-integrated form of (23), we can calculate the total crest passage rate (denominator term) over the spectral peak region, which we define by $c_p - \Delta c / 2 < c < c_p + \Delta c / 2$, where $|\Delta c / c_p| < 1$. The details are given in Appendix, where (A6) gives

$$\Pi(c_p) = \chi g / (2\pi c_p^3).$$

Since

$$A(c_p) = \Pi(c_p) * Pr(\tilde{\sigma}_p)$$

it follows that

$$A(c_p) = (\chi g / 2\pi c_p^3) * Pr(\tilde{\sigma}_p) \quad (28)$$

Using (26)–(28) gives

$$b_p = 2 \frac{g^3 S_{ds}^{loc}(k_p)}{c_p^8 A(c_p)} \quad (29)$$

$$b_p = \frac{4\pi g^2 S_{ds}^{loc}(k_p)}{\chi c_p^5 Pr_{br}(\tilde{\sigma}_p)}$$

with $Pr_{br}(\tilde{\sigma}_p)$ given by (24). Therefore, (28) and (29) together with (24) provide the breaking crest length spectral density/unit area, $A(c_p)$, and breaking strength, b_p , for the spectral peak waves at any stage of the evolution, using the computed wave height spectrum and dissipation rate spectrum from the model.

Integrating various c -moments of $A(c)$ over the assumed spectral peak bandwidth gives several key quantities of interest associated with breaking waves. These include the mean passage rate of the dominant breakers past a fixed point (first moment), kinematic breaking wave stress imparted to the upper ocean (fourth moment), and energy dissipation rate (fifth moment). See Section 6 in Phillips (1985) for further details.

3.6. Full bandwidth computation of duration-limited wind wave evolution

Computations of the directional wave spectrum were made for the full spectral bandwidth typically covering 0.02–4.0 Hz, depending on the wind speed, using the source terms described in Sections 3.2–3.4. In this paper we focus on the case of a steady forcing wind speed of $U_{10} = 12$ m/s, noting that during periods 1 and 3 of FAIRS annotated in Fig. 1, the prevailing mean wind speed $U_{10} \sim 12$ m/s was blowing for 6–8 h prior to the wave measurements reported here.

Of particular interest is benchmark D, a comparison of observed and forecast breaking wave properties at the spectral peak during developing seas. Such a comparison has not been undertaken previously. Not only does this provide a tighter constraint on the form of the spectral dissipation rate source term, but it has the additional benefit of reducing the uncertainty in the form of S_{in} , as explained below.

4. Results and discussion

4.1. Validations against standard benchmarks

We validated our model results for non-dimensional wave energy and spectral peak frequency against the duration-limited data trend curve given by Young (1999, §5.3.4) (benchmark A in Section 2.2). The results are shown in Fig. 4a, where it is seen that our model closely reproduces the trends of the observations, including the transition to swell for very old wind seas. The evolution curves for stronger wind forcing out to hurricane strength continue to show a very similar close conformity to Young's curves, with no change in any of the source term parameterisations. The performance of these source terms in more complex sea states is left to a future study.

Also, the behaviour of the integrated source terms in Fig. 4b shows that the integrated S_{in} and S_{ds} terms initially increase then decrease towards large durations. They asymptote towards each

other as the wind sea matures. The integrated S_{nl} term is zero for all times, as required.

An important validation check can be made on the total wave energy dissipation rate in the water column, reflected in the integrated S_{ds} curve in Fig. 4b. During the FAIRS experiment, Gemmrich and Farmer (2004) made unique measurements of the dissipation rate just below the sea surface in the presence of the breaking waves. Using the Craig and Banner (1994) model to extrapolate over the wave boundary layer and mixed layer, they estimated the total dissipation rate during period 2 was about $6.5 \times 10^{-4} \text{ m}^3 \text{ s}^{-3}$. The corresponding level forecast for period 1 by our model is $5.2 \times 10^{-4} \text{ m}^3 \text{ s}^{-3}$, decreasing to $4.3 \times 10^{-4} \text{ m}^3 \text{ s}^{-3}$ for the mature seas in period 3.

Given the numerous uncertainties in the parameters input to the Craig and Banner (1994) model, we also used the observational results of Fig. 5 in Terray et al. (1996) to estimate the total dissipation rate during FAIRS. For the evolving conditions of period 1, $u_*^a/c_p \approx 0.048$, hence $\bar{c}/c_p \approx 0.23$, while for the mature period 3 waves, $u_*^a/c_p \approx 0.037$, hence $\bar{c}/c_p \approx 0.14$. The energy flux from the air to the water is then given by their Eq. (5):

$$F_e \approx \tau_a \bar{c} / \rho_{\text{water}} \quad (30)$$

F_e closely approximates the turbulent energy flux from the breaking waves to turbulence in the water column. According to the Terray et al. (1996) data compilation, for the observational periods 1 and 3, the estimated integrated breaking wave energy fluxes (or total dissipation rates) are, respectively, 6.4×10^{-4} and $4.9 \times 10^{-4} \text{ m}^3 \text{ s}^{-3}$.

While our computed dissipation rates are marginally lower than the observational estimates, they are arguably within the observational uncertainty bounds. Given the intrinsic difficulty in making these measurements, we were reassured by this aspect of the model validation. The utility of this validation criterion motivates the acquisition of further dissipation rate data and simultaneous wind input data, especially for higher wind speeds.

The results for the additional benchmarks B in Section 2.2 are shown in Figs. 5 and 6. These computed spectral measures are in close accord with available data.

Due to the specialised techniques and instrumentation needed for these wavenumber domain measurements, these spectral properties are not routinely measured. The saturation and smoothed normalised saturations curves, transformed to the frequency domain, are in broad agreement with the measurements of Gemmrich et al. (2008), especially around the spectral peak. In Fig. 5c, it is seen that the directional spreading curves are consistent with Hwang et al. (2000) in the spectral peak region (out to $6 k_p$, the upper bound of their measurements), including the lobed (bi-model) structure. The mean directional spreading angle, defined in Section 3.4, is shown in Fig. 5d. It shows a gradual broadening from about 20° at the spectral peak, out to about 40° for higher wavenumbers. This varies with wave age with a gradual reduction towards older seas.

Fig. 6 shows another spectral tail diagnostic that has been measured frequently. This is the one-dimensional wavenumber transect spectrum. Fig. 6 shows a comparison with Melville and Matusov (2002) for mature wind seas. The computed spectrum, for wave age 1.2 and $U_{10} = 12$ m/s, closely matches the observed spectrum. According to Melville and Matusov (2002), the latter shows very little variation for U_{10} between 7 and 13 m/s.

The remaining benchmark C is concerned with the relative size of wave-induced stress level in the computational domain. The sum of the non-breaking and breaking wave-coherent wind stress components and the viscous tangential stress equals the total wind stress, which was measured in the FAIRS experiment and is shown above in the lower panel of Fig. 1.

The measured wind stress from FAIRS (see Fig. 1) is equivalent to a drag coefficient of 1.6×10^{-3} for developing seas during period 1 (wave age ~ 0.9) and 1.3×10^{-3} for the mature wind seas (wave

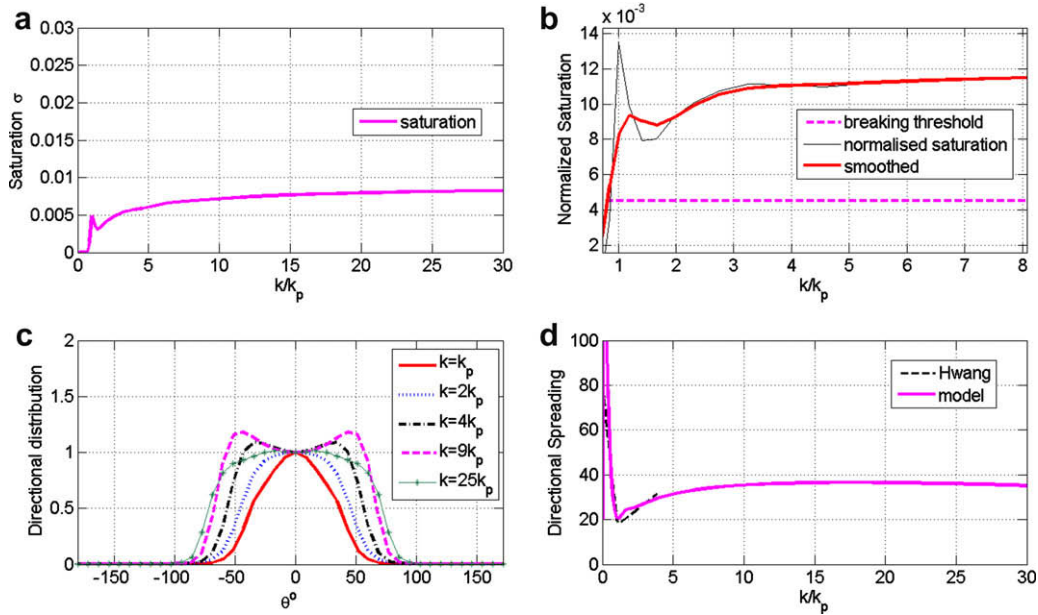


Fig. 5. The wind and wave conditions are $U_{10} = 12$ m/s and inverse wave age $U_{10}/c_p = 1.21$. The upper two panels show the spectral saturation (the azimuth averaged fourth moment of the wavenumber spectrum). (a) How the saturation changes with distance from the spectral peak. (b) The corresponding behaviour of the saturation normalised by the corresponding mean directional spreading width, and the 5-point smoothed normalised saturation. The directional spreading properties are seen in the lower two panels. The weakly bimodal angular spreading distributions at various distances from the spectral peak are seen in the left panel, while the right panel shows how the mean spreading width varies with distance from the spectral peak. The angle shown is the half-width in degrees. The data in (d) is from Hwang et al. (2000).

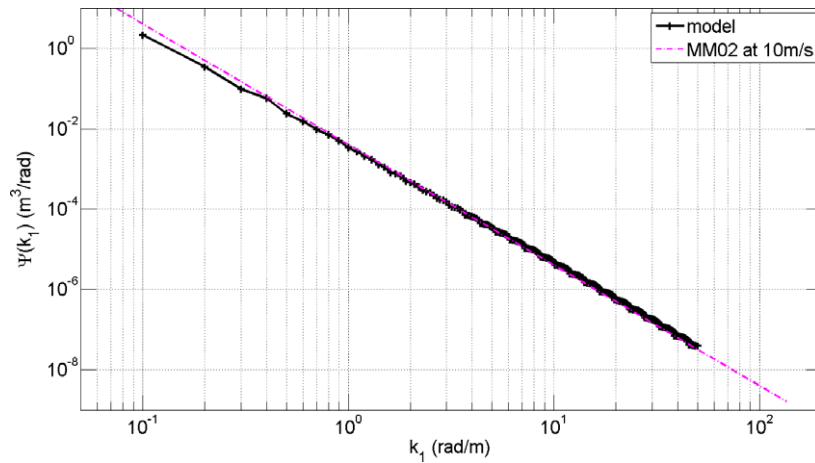


Fig. 6. One-dimensional (k_1) transect spectrum in the upwind-downwind direction for a mature wind sea ($c_p/U_{10} \sim 1.2$), showing a close correspondence with the measured k_1^{-3} data trend of Melville and Matusov (2002) (indicated MMO2), measured for very old wind seas with $U_{10} \sim 10$ m/s. Their data showed very little variation in the spectral level over the 8–13 m/s wind speed range.

age ~ 1.2) during period 3. The model results in Fig. 7 closely agree with these observed levels of the total drag coefficient. However, there is presently no field data available to validate the modelled component stress values.

4.2. Wave breaking forecast validation

From the primary model output of the components of the spectral dissipation rate S_{ds} [see Eq. (17)] and normalised saturation $\bar{\sigma}$ at any given stage of evolution, the predicted spectral peak values of $\mathcal{A}(c)$ and breaking strength b are calculated from (24), (28), and (29). The goal of this novel and challenging aspect of the model validation is to reproduce the observed breaking crest length spectral density \mathcal{A} and breaking strength b for the dominant waves. There is only one non-zero validation data point in FAIRS. This arises from the evolution during period 1 where the inverse wave age $U_{10}/$

$c_p = 1.09$. In period 3, the normalised saturation has fallen below the breaking threshold at the spectral peak, therefore no breaking at the spectral peak is predicted, and indeed, none was observed.

A detailed comparison was made of the observed and model results for breaking of the dominant wind waves in period 1. For these conditions ($U_{10}/c_p \sim 1.09$), the observed breaking probability was 0.05, assuming a spectral peak breaking speed of 0.85 of the corresponding linear phase speed (Melville and Matusov, 2002; Gemmrich et al., 2008). The computed smoothed normalised spectral peak saturation was $\bar{\sigma} = 0.0062$, giving a breaking probability $Pr_{br} = 0.056$, which corresponds closely to the observed breaking probability. For the mature sea state in period 3, the model predicts zero breaking at the spectral peak, as the normalised spectral saturation was below the threshold. These conclusions were also confirmed in the observed histograms of breaking wave fraction against speed c shown in Fig. 2.

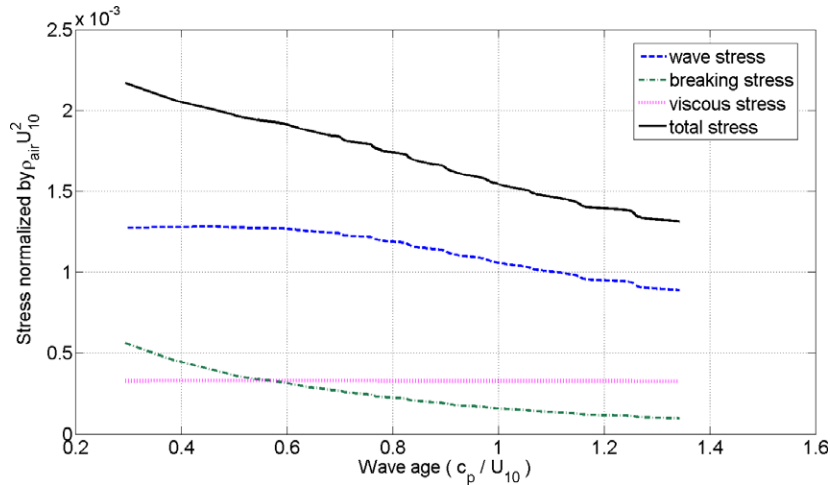


Fig. 7. Behaviour of the normalised total wind stress, wave-coherent wind stress, breaking-induced wind stress and viscous tangential stress as the wind sea ages for $U_{10} = 12$ m/s. The viscous stress extrapolates the estimate by Banner and Peirson (1998).

Reference to Fig. 8 shows that the observed dominant wave crest length spectral density for period 1 was $\Lambda(c_p) \sim 1.0 \times 10^{-4}$. For comparison, based on (28) and a spectral peak breaking speed of 0.85 of the corresponding linear phase speed, the modelled spectral peak level of $\Lambda(c_p) \sim 1.05 \times 10^{-4}$ is plotted in Fig. 8, indicating a very close correspondence with the observed value.

In regard to comparing observed and calculated values for the breaking strength b , there are no available verifying field data to validate our modelled values of b for the spectral peak waves. This

is because present measurement methods do not provide a spectral resolution of the dissipation rate S_{ds} .

A mean breaking strength $\langle b \rangle \sim 5 \times 10^{-5}$ for period 1 was reported by Gemmrich et al. (2008) under the assumption that b is constant across the whole spectrum. This strong assumption remains to be substantiated when spectral measurements of S_{ds} become available. Nevertheless, if this assumption is made, the corresponding modelled $\langle b \rangle$ value can be calculated from the integral of (22) over the wave spectrum, using the calculated S_{ds}^{loc}

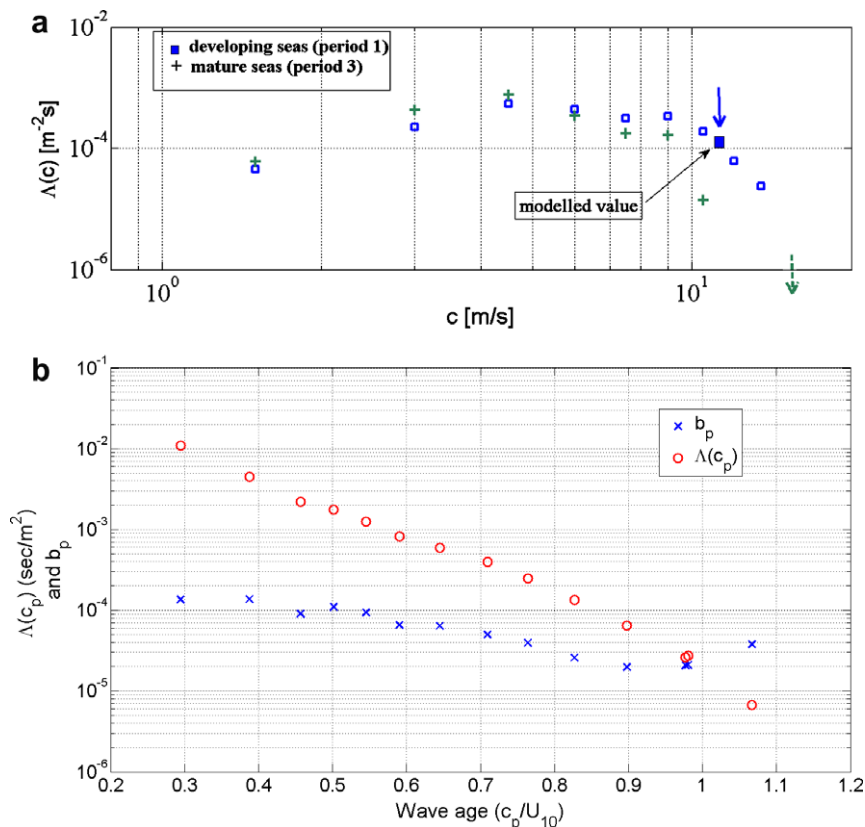


Fig. 8. (a) Measured breaking wave crest length spectral density $\Lambda(c)$ for period 1 (squares) and period 3 (+) during the evolution for $U_{10} = 12$ m/s. The vertical arrows indicate the spectral peaks corresponding to the wave age conditions during periods 1 and 3, where the spectral peak speeds were 11 and 15.5 m/s, respectively. The modelled value of $\Lambda(c_p)$ is indicated. (b) Modelled variation of the spectral density $\Lambda(c_p)$ of breaking crest length per unit area and breaking strength b_p for the spectral peak waves with wave age c_p/U_{10} , for $U_{10} = 12$ m/s.

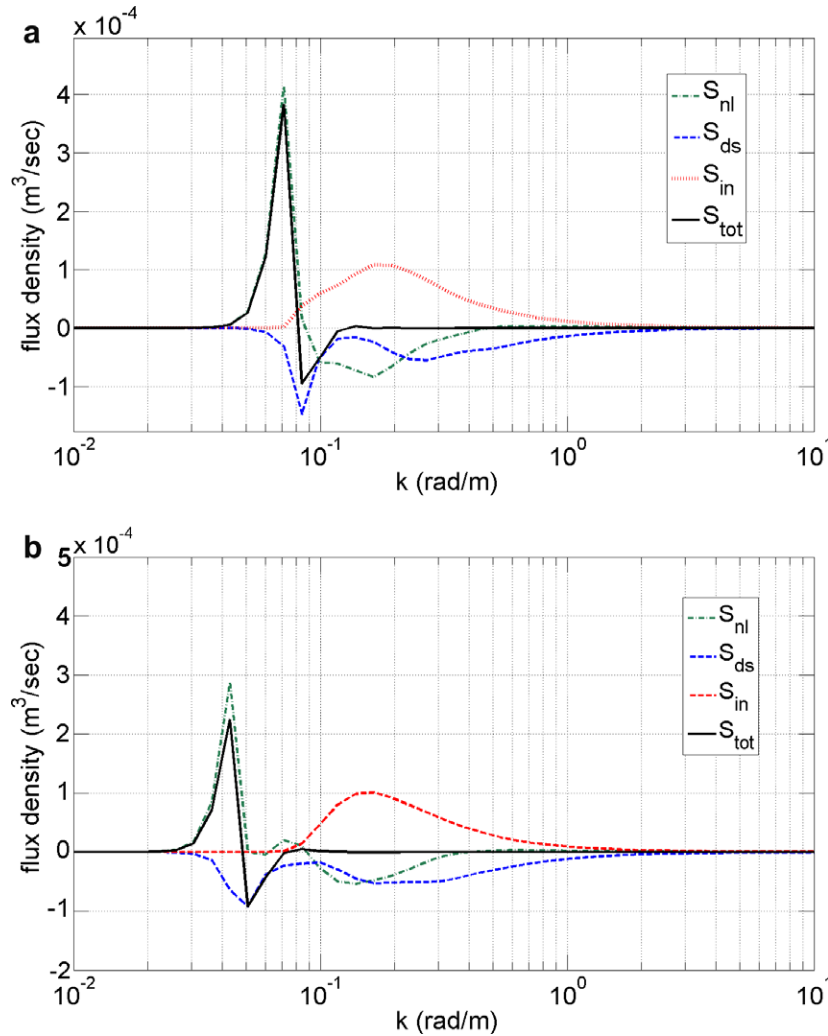


Fig. 9. Source term balance for developing seas (inverse wave age $U_{10}/c_p \sim 1.09$) in period 1 (left panel) and maturing seas (inverse wave age $U_{10}/c_p \sim 0.81$) in period 3 (right panel). Note that even for period 1, the spectral peak dissipation rate is considerably larger than the wind input, as discussed in the text.

spectrum, together with $\mathcal{A}(c) = \Pi(c) Pr_{br}(c)$ estimated from (A5) and (24), using the normalised saturation calculated from the wave model output. Also, χ was calculated from an analysis of period 1 wave height time series data, using our Riding Wave Removal code (Banner et al., 2002), with χ showing an approximately $(f/f_p)^{-1}$ behaviour. The resultant value of $\langle b \rangle$ was calculated as 5.5×10^{-5} .

Overall, these results show a very close correspondence between the observed and modelled \mathcal{A} properties of the waves in the spectral peak band, and mean value of breaking strength $\langle b \rangle$, under the assumption that b is uniform across the spectrum.

Underlying the transition from period 1 to period 3 is the source term balance, shown in Fig. 9. A noteworthy feature is that the level of the wind input to the dominant waves decreases to well below the dissipation rate as the wave speed approaches the wind speed. However, the dominant wave saturation level (and steepness) remains sufficiently large for the breaking to occur through nonlinear interactions, e.g. weakly nonlinear wave group modulations as reported in Banner and Peirson (2007), augmented by the non-local dissipation rate.

5. Conclusions

This research provides new forms for both the wind input and dissipation source terms for spectral wave models, as well as a to-

tally new formulation for crest length spectral density per unit area and strength of the spectral peak breaking waves.

We describe the development of consistent dissipation rate and wind input spectral source terms for wind-generated waves, and their validation in duration-limited evolution in conjunction with the ‘exact’ nonlinear spectral transfer source term. The dissipation rate term is a substantial reformulation of the Alves and Banner (2003) saturation threshold form. Following an extensive evaluation of several popular wind input source terms, we adopted a wind input term that closely follows the Janssen (1991) formulation, but with sheltering introduced to dampen the input to the shorter waves.

In addition, our new framework for forecasting breaking properties (crest length spectral density per unit area and breaking strength) of the dominant waves using standard wave model outputs provide accurate forecasts for the limited breaking data available for both developing and mature wind seas. Further validation against data will be made as it becomes available.

Our validation procedure examined model performance for a comprehensive range of wave spectral properties: duration-limited evolution of wave energy and peak frequency, one-dimensional wavenumber spectrum, spectral directional spreading, together with the computed atmospheric drag coefficient and dissipation rate in the water column.

A novel element is included in the validation, associated with the recent availability of spectral wave breaking data gathered synchronously with the usual wind and wave height data during the recent FAIRS field investigation. This data provided an additional strong constraint on the wind input and dissipation rate source terms, in addition to refining our understanding of the evolution of wind waves. In evaluating different forms for the wind input term, we found that the spectral distribution of the wind input is crucial for the model to be able to deliver accurate forecasts of breaking properties. In particular, if the wind input is too weak in the spectral peak region during the growth phase, the observed wave energy growth may be reproduced, but the model cannot reproduce the observed dominant wave breaking levels. These additional constraints set a new benchmark in restricting ‘allowable’ forms of the major source terms in future model development.

Overall, with our matched source terms, the model was able to closely reproduce the available data for each of our validation criteria. The focus in this paper was on the model framework and its performance for a wind forcing strength of 12 m/s. In a companion paper, we describe results for wind speeds ranging from 6 up to 60 m/s. Using more accurate forms of the wind input source term and energy dissipation rate will benefit both the reliability and utility of wave forecasts, especially with the contemporary goal of coupling wave models to upper ocean circulation and atmospheric models. This study highlights the need to refine present observational knowledge of the wave boundary layer, in addition to the wind input source term.

Acknowledgements

The authors gratefully acknowledge the research support for this project received from the Office of Naval Research under the CBLAST Departmental Research Initiative, and from the Australian Research Council. Special thanks are due to Johannes Gemmrich for providing the FAIRS breaking wave observational results during the course of this investigation and to Don Resio for access to his S_{nl} code, and to Ekaterini Kriezis for her participation in the early model development.

Appendix A

A.1. Derivation of an expression for the spectral density of total crest length per unit area $\Pi(c)$

We investigate the validity of the form

$$\Pi(c) = \chi(c)g/2\pi c^3 \tag{A1}$$

for the spectral density of total crest length/unit area for an ensemble of gravity surface waves.

The dimensions of $\Pi(c)$ are T/L^2 . From a dimensionally consistent grouping of the parameters in the problem, g and wave speed c , it is evident that

$$\Pi(c) = Ag/c^3 \tag{A2}$$

where A is a constant to be determined. We first determine A for the limiting case of a unimodal sinusoidal wave of frequency f_0 . For this case, the mean crest length per unit area is easily seen to be $1/\lambda$, where λ is the corresponding wave length.

We apply the results of Eq. (13) for generalised functions in Lighthill (1962):

$$\lim_{n \rightarrow \infty} \int_{-\infty}^{\infty} f_n(ax + b)F(x)dx = \frac{1}{|a|} \lim_{n \rightarrow \infty} \int_{-\infty}^{\infty} f_n(x)F\left(\frac{x-b}{a}\right) dx \tag{A3}$$

to Eq. (A2), choosing f_n as sequence that represents the Dirac delta function $\delta(x)$, and $F = \Pi(c)$ as specified in (A2).

We evaluate A from the relation

$$\int_{-\infty}^{\infty} \delta\left(\frac{c}{c_0} - 1\right) \Pi(c) dc = \frac{1}{\lambda_0} \tag{A4}$$

Setting $a = 1/c_0$ and $b = -1$ in (A3), and substituting (A2), the integral on the left transforms to

$$c_0 \int_{-\infty}^{\infty} \delta(c) Ag/((c + 1)c_0)^3 dc = Ac_0 g \frac{1}{c_0^3} = Ag \frac{1}{c_0^2}$$

after using the sifting property of $\delta(c)$.

Hence equating this to $1/\lambda$, we obtain $A = 1/2\pi$ since for gravity water waves, $c^2 = g/k = g\lambda/2\pi$.

Therefore, the form

$$\Pi(c) = g/2\pi c^3 \tag{A5}$$

for the crest length spectral density per unit area proposed in (A1) gives the correct result for the mean crest length/unit area for the limiting case of a monochromatic wave mode.

Further, it is easily verified using the same methodology that the first moment of the proposed spectral density, $c\Pi(c) = g/2\pi c^2$, yields $f_0 (= g/2\pi c_0)$ for this limiting case, which is the correct mean passage rate of wave crests past a fixed point.

For the present application to a spectral peak wave bandwidth of open ocean wind waves, with a possible directional distribution and spatio-temporal intermittency of waves of any given scale, we investigate the application of the proposed form (A4) to the spectral peak wave passage rate as follows:

We define the spectral peak region by $c_l < c_p < c_u$, where c_l and c_u are nominated lower and upper bounds for the spectral peak region.

We seek to investigate the estimation of the mean wave crest passage rate past a fixed point in this spectral peak bandwidth by integrating over the spectral peak bandwidth the first moment of $\Pi(c)$ given by (A5) modified for the possible directionality and/or spatio-temporal intermittency factor, represented by $\chi_p = \chi(c_p)$.

It is easily seen that the mean passage rate of all wave crests is given by

$$\int_{c_l}^{c_u} c\Pi(c) dc = \int_{c_l}^{c_u} c\chi(c) \frac{g}{2\pi c^3} dc = \int_{f_l}^{f_u} \chi(f) df \tag{A6}$$

Assuming a mean value χ_p for the nominal spectral peak region taken as $[0.7f_p, 1.3f_p]$ in (A6), the mean passage rate of spectral peak waves is $0.6\chi_p f_p$.

From the FAIRS wave data, the measured total crest passage rate for this nominal bandwidth at the spectral peak using the Riding Wave Removal method (Banner et al., 2002) was found to be $0.62f_p$ for the same proposed nominal spectral peak bandwidth $[0.7f_p, 1.3f_p]$. Thus, for this data set, $\chi_p = \chi(c_p) \sim 1.0$.

From these results, the expected value, $\langle \Pi(c_p) \rangle$, of $\Pi(c)$ averaged over this spectral peak region, can be defined as

$$\langle \Pi(c_p) \rangle \approx 0.6g/(2\pi c_p^3) \tag{A7}$$

with the corresponding mean passage rate defined in (A6) given by $c_p \langle \Pi(c_p) \rangle$.

It should be noted that the factor χ_p , or more generally, $\chi(c)$, will depend on the structure of the wave field and the bandwidth chosen. As long as the corresponding bandwidth is used to identify the breakers and gives a sufficient breaker count, no difficulties should arise in quantifying the breaking probability for that scale.

References

Alves, J.H., Banner, M.L., 2003. Performance of a saturation-based dissipation source term for wind wave spectral modelling. *J. Phys. Oceanogr.* 33, 1274–1298.
 Ardhuin, F., Jenkins, A.D., 2006. On the interaction of surface waves and upper ocean turbulence. *J. Phys. Oceanogr.* 36, 551–557.

- Babanin, A.V., Banner, M.L., Young, I.R., Donelan, M.A., 2007. Wave follower field measurements of the wind input spectral function. Part III: Breaking wave enhancement. *J. Phys. Oceanogr.* 37, 2764–2775.
- Banner, M.L., Babanin, A.V., Young, I.R., 2000. Breaking probability for dominant waves on the sea surface. *J. Phys. Oceanogr.* 30, 3145–3160.
- Banner, M.L., Jones, I.S.F., Trinder, J.C., 1989. Wavenumber spectra of short gravity waves. *J. Fluid Mech.* 198, 321–344.
- Banner, M.L., Chen, W., Walsh, E.J., Jensen, J.B., Lee, S., Fandry, C.B., 1999. Results from the SOWEX experiment. Part 1: Overview and mean results. *J. Phys. Oceanogr.* 29, 2130–2145.
- Banner, M.L., Gemmrich, J.R., Farmer, D.M., 2002. Multiscale measurements of ocean wave breaking probability. *J. Phys. Oceanogr.* 32, 3364–3375.
- Banner, M.L., Peirson, W.L., 1998. Tangential stress beneath wind-driven air–water interfaces. *J. Fluid Mech.* 364, 115–145.
- Banner, M.L., Peirson, W.L., 2007. Wave breaking onset and strength for two-dimensional deep water waves. *J. Fluid Mech.* 585, 93–115.
- Belcher, S.E., Hunt, J.C.R., 1993. Turbulent shear flow over slowly moving waves. *J. Fluid Mech.* 251, 109–148.
- Br on, F.M., Henriot, N., 2006. Spaceborne observations of ocean glint reflectance and modeling of wave slope distributions. *J. Geophys. Res.* 111, C06005.
- Cox, C.S., Munk, W.H., 1954. Measurements of the roughness of the sea surface from photographs of the sun glitter. *J. Opt. Soc. Am.* 44, 838–850.
- Craig, P.D., Banner, M.L., 1994. Modelling wave-enhanced turbulence in the ocean surface layer. *J. Phys. Oceanogr.* 24, 2546–2559.
- Donelan, M.A., Longuet-Higgins, M.S., Turner, J.S., 1972. Whitecaps. *Nature* 239, 449–451.
- Donelan, M.A., 1998. Air–water exchange processes. In: Imberger, J. (Ed.), *Physical Processes in Oceans and Lakes*. AGU Coastal and Estuarine Studies 54, 19–36.
- Gemmrich, J.R., Farmer, D.M., 2004. Near-surface turbulence in the presence of breaking waves. *J. Phys. Oceanogr.* 34, 1067–1086.
- Gemmrich, J.R., Banner, M.L., Garrett, C., 2008. Spectrally resolved energy dissipation and momentum flux of breaking waves. *J. Phys. Oceanogr.* 38, 1296–1312.
- Hara, T., Belcher, S.E., 2002. Wind forcing in the equilibrium range of wind-wave spectra. *J. Fluid Mech.* 470, 223–245.
- Holthuijsen, L.H., Herbers, T.H.C., 1986. Statistics of breaking waves observed as whitecaps in the open sea. *J. Phys. Oceanogr.* 16, 290–297.
- Hsiao, S.V., Shemdin, O.H., 1983. Measurements of wind velocity and pressure with a wave follower during MARSEN. *J. Geophys. Res.* 88, 9841–9849.
- Hwang, P.A., Wang, D.W., Walsh, E.J., Krabill, W.B., Swift, R.W., 2000. Airborne measurements of the wavenumber spectra of ocean surface waves. Part II: Directional distribution. *J. Phys. Oceanogr.* 30, 2768–2787.
- Hwang, P.A., Wang, D.W., 2004. Field measurements of duration-limited growth of wind-generated ocean surface waves at young stage of development. *J. Phys. Oceanogr.* 34, 2316–2326.
- Janssen, P.A.E.M., 1991. Quasi-linear theory of wind-wave generation applied to wave forecasting. *J. Phys. Oceanogr.* 21, 1631–1642.
- Komen, G.J., Cavaleri, L., Donelan, M.A., Hasselmann, K., Hasselmann, S., Janssen, P.A.E.M., 1994. *Dynamics and Modelling of Ocean Waves*. Cambridge University Press, Cambridge. 532 pp.
- Lighthill, M.J., 1962. *Introduction to Fourier Analysis and Generalised Functions*, CUP. 79 pp.
- Makin, V.K., Kudryavtsev, V.N., 2001. Coupled sea surface-atmosphere model. 1. Wind over waves coupling. *J. Geophys. Res.* 104, 7613–7623.
- Melville, W.K., Matusov, P., 2002. Distribution of breaking waves at the ocean surface. *Nature* 417, 58–63.
- Melville, W.K., 1994. Energy dissipation by breaking waves. *J. Phys. Oceanogr.* 24, 2041–2049.
- Miles, J.W., 1957. On the generation of surface waves by shear flows. *J. Fluid Mech.* 3, 185–204.
- Phillips, O.M., 1985. Spectral and statistical properties of the equilibrium range in wind-generated gravity waves. *J. Fluid Mech.* 156, 505–531.
- Phillips, O.M., Posner, F.L., Hansen, J.P., 2001. High resolution radar measurements of the speed distribution of breaking events in wind-generated ocean waves. Surface impulse and wave energy dissipation rates. *J. Phys. Oceanogr.* 31, 450–460.
- Plant, W.J., 1982. A relation between wind stress and wave slope. *J. Geophys. Res.* 87, 1961–1967.
- Resio, D., Perrie, W., 2008. A two-scale approximation for efficient representation of nonlinear energy transfers in a wind wave spectrum. Part 1: Theoretical development. *J. Phys. Oceanogr.* 38 (12), 2801–2816.
- Restrepo, J.M., 2007. Wave breaking dissipation in a wave-driven circulation. *J. Phys. Oceanogr.* 37, 1749–1763.
- Song, J., Banner, M.L., 2002. On determining the onset and strength of breaking for deep water waves. Part 1: Unforced irrotational wave groups. *J. Phys. Oceanogr.* 32, 2541–2558.
- Snyder, R.L., Dobson, F.W., Elliott, J.A., Long, R.B., 1981. Array measurements of atmospheric pressure fluctuations above surface gravity waves. *J. Fluid Mech.* 102, 1–59.
- Terray, E.A., Donelan, M.A., Agrawal, Y.C., Drennan, W.M., Kahma, K.K., Williams III, A.J., Hwang, P.A., Kitaigorodskii, S.A., 1996. Estimates of kinetic energy dissipation under breaking waves. *J. Phys. Oceanogr.* 26, 792–807.
- Teixeira, M.A.C., Belcher, S.E., 2002. On the distortion of turbulence by a progressive surface wave. *J. Fluid Mech.* 458, 229–267.
- Tian, Z., Perlin, M., Choi, W., 2008. Evaluation of a deep-water breaking criterion. *Phys. Fluids* 20, 066604. doi:10.1063/1.2939396.
- Tolman, H.L., Chalikov, D., 1996. Source terms in a third-generation wind wave model. *J. Phys. Oceanogr.* 26, 2497–2518.
- Tracy, B.A., Resio, D.T., 1982. Theory and calculation of the nonlinear energy transfer between sea waves in deep water. WIS Rept. 11, US Army Engineers Waterway Experiment Station.
- Yan, L., 1987. An improved wind input source term for third generation ocean wave modelling. Royal Netherlands Meteorological Institute Scientific Rep. WR-87-8, 10 pp.
- Young, I.R., 1999. *Wind Generated Ocean Waves*. Elsevier. 288 pp.